Crystallisation-Induced Emission Enhancement in Zn(II) Schiff Base Complexes with a Tuneable Emission Colour

GOLDING, Declan J. L. <http://orcid.org/0000-0001-8704-8741>, CARTER, Nicholas, ROBINSON, David <http://orcid.org/0000-0003-2760-7163> and FITZPATRICK, Anthony J. <http://orcid.org/0000-0001-9436-8129>

Published version

GOLDING, Declan J. L., CARTER, Nicholas, ROBINSON, David and FITZPATRICK, Anthony J. (2020). Crystallisation-Induced Emission Enhancement in Zn(II) Schiff Base Complexes with a Tuneable Emission Colour. Sustainability, 12 (22), e9599.

sustainability

MDPI

Article

Crystallisation-Induced Emission Enhancement in Zn(II) Schiff Base Complexes with a Tuneable Emission Colour

Declan J. L. Golding [1], Nicholas Carter [1], David Robinson [1] and Anthony J. Fitzpatrick [2,*]

[1] School of Science and Technology, Nottingham Trent University, Clifton Lane, Nottingham NG11 8NS, UK; Declan.golding2016@my.ntu.ac.uk (D.J.L.G.); nicholas.carter@ntu.ac.uk (N.C.); david.robinson@ntu.ac.uk (D.R.)

[2] Department of Biosciences and Chemistry, Sheffield Hallam University, Sheffield S1 1WB, UK

* Correspondence: anthony.fitzpatrick@shu.ac.uk

Received: 15 October 2020; Accepted: 16 November 2020; Published: 18 November 2020

Abstract: Four Zn(II) Schiff base complexes that exhibit crystallisation-induced emission enhancement (CIEE) are presented. There is an intermolecular dimerisation through the hydrogen bonding of the mixed phenol/phenolate donors. The choice of ligand also determines the emission wavelength. The complexes have been investigated using experimental and theoretical techniques.

Keywords: crystallisation-induced emission; luminescence; coordination chemistry; Schiff base; inorganic

1. Introduction

The interaction of light with organic molecules and transition metal coordination complexes is becoming an increasingly widely studied area. Applications in organic light-emitting diodes (OLEDs) [1], photocatalysis [2] and fluorescence-based sensors [3–5] have all been investigated. The luminescent character of such complexes can vary greatly when moving from solution to the solid state. Usually, the vast majority of compounds that exhibit fluorescence have higher photoemission in solution than in the solid state, due to aggregation-caused quenching (ACQ) [6–8]. However, certain organic luminophores that have freely-rotating groups, e.g., alkyl chains, show higher levels of emission when aggregation occurs, termed aggregation-induced emission (AIE) [9]. Upon aggregation, the freely rotating groups, which in solution lead to nonradiative relaxation, are restricted and enhanced emission is observed. AIE has been observed in both organic systems as well as metal-containing systems where there is flexibility around the luminophore. Crystallisation-induced emission enhancement (CIEE) is a phenomenon similar to AIE, where the compound emits weakly in solution or in a disordered/amorphous solid but emits very strongly when in crystalline form (Figure 1) [10–17]. As with AIE, CIEE is caused by the restriction of freely rotating groups in the molecule resulting in enhancement of the efficiency of fluorescence or photoluminescence [18].

Numerous examples of Schiff base derived ligands exist which show interesting luminescent properties with d^{10} Zn(II) [19–25]. This is due to both the simplicity of synthesis and ease of variation of Schiff base ligands in general. Zinc complexes are of interest as they are earth-abundant and many of the interesting applications for optics currently use rare earth metals as the luminescent ion.

Here we present four novel Zn(II) pseudo-octahedral coordination complexes that exhibit CIEE. The complexes employed are based on the Schiff base condensation of 2-hydrazinopyrazine with a variety of substituted salicylaldehydes followed by coordination of zinc nitrate to yield complexes **1**–**4** (Scheme 1).

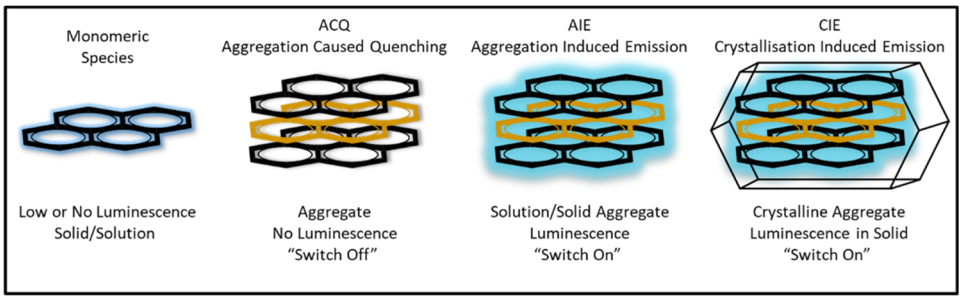

Figure 1. Representative diagrams for (left–right) luminesce in a monomer, aggregation-caused quenching, aggregation-induced emission and crystallisation-induced emission.

L1, R = H
L2, R = 3-OMe
L3, R = 4-NEt_2
L4, R = 5-Cl

Complex **1**, $[Zn(L1)(HL1)]NO_3$
Complex **2**, $[Zn(L2)(HL2)]NO_3$
Complex **3**, $[Zn(L3)(HL3]NO_3 \cdot 3H_2O$
Complex **4**, $[Zn(L4)(HL4)]NO_3$

Scheme 1. Synthesis of complexes **1**–**4**.

2. Materials and Methods

All chemicals were ordered from either Sigma-Aldrich (Merck) or Fluorochem and used without further purification. All solid-state fluorescence spectra were obtained using a TECAN infinite M200 Pro with an excitation of 405 nm. All synthesis was carried out under aerobic benchtop conditions.

2.1. Synthesis

Complex **1**, $[Zn(L1)(HL1)]NO_3 \cdot H_2O$

An amount of 0.110 g (1 mmol) of 2-hydrazinopyrazine was added to 0.106 mL (1 mmol) of salicylaldehyde in 20 mL of 1:1 methanol/acetonitrile and stirred for 10 min. To this 0.149 g (0.5 mmol) of $Zn(NO_3)_2 \bullet 6H_2O$ was added and stirred for 20 min and the solution was filtered. Yellow crystals were isolated after several days of slow solvent evaporation. Isolated Yield 105 mg, 19%.

IR (cm^{-1}): 3207, 3049, 1617, 1537, 1515, 1455, 1285, 1207, 1153, 749.
Elemental Analysis: Theory (Found); C, 46.13 (45.89); H, 3.70 (3.83); N, 22.01 (22.15).
^1H NMR (400 MHz, DMSO-D_6) δ 11.23 (s, 1H), 10.39 (s, 1H), 8.45 (s, 1H), 8.34 (s, 1H), 8.11 (s, 1H), 7.96 (t, *J* = 8.3 Hz, 1H), 7.69–7.61 (m, 1H), 7.22–7.15 (m, 1H), 6.86 (s, 2H).

Complex **2**, $[Zn(L2)(HL2)]NO_3 \cdot H_2O$

An amount of 0.110 g (1 mmol) of 2-hydrazinopyrazine was added to 0.152 g (1 mmol) of 3-methoxysalicylaldehyde in 20 mL of 1:1 methanol/acetonitrile and stirred for 10 min. To this 0.149 g (0.5 mmol) of $Zn(NO_3)_2 \bullet 6H_2O$ was added and stirred for 20 min and the solution was filtered. Yellow/orange crystals were isolated after several days of slow solvent evaporation. Isolated Yield 84 mg, 13.5%.

IR (cm^{-1}): 3199, 3091, 3037, 1617, 1537, 1515, 1457, 1388, 1340, 1239, 829, 773.
Elemental Analysis: Theory (Found); C, 45.55; (45.54) H, 3.98 (3.77); N, 19.92 (20.37).
^{1}H NMR (400 MHz, DMSO-D_6) δ 11.55 (s, 1H), 8.52 (d, *J* = 1.2 Hz, 1H), 8.42 (s, 1H), 8.17–8.13 (m, 1H), 8.01 (d, *J* = 2.8 Hz, 1H), 7.36 (dd, *J* = 7.9, 1.4 Hz, 1H), 6.97 (dd, *J* = 8.1, 1.4 Hz, 1H), 6.82 (t, *J* = 7.9 Hz, 1H), 3.81 (s, 3H).

Complex **3**, $[Zn(L3)(HL3)]NO_3 \cdot H_2O$

An amount of 0.110 g (1 mmol) of 2-hydrazinopyrazine was added to 0.193 g (1 mmol) of 4-diethylamino salicylaldehyde in 20 mL of 1:1 methanol/acetonitrile and stirred for 10 min. To this 0.149 g (0.5 mmol) of $Zn(NO_3)_2 \bullet 6H_2O$ was added and stirred for 20 min and the solution was filtered. Orange crystals were isolated after several days of slow solvent evaporation. Isolated Yield 154 mg, 22.5%.

IR (cm^{-1}): 3194, 3039, 2968, 1603, 1537, 1515, 1455, 1284, 1138, 1015, 820, 766.
Elemental Analysis: Theory (Found); C, 50.39 (50.36); H, 5.50 (5.77); N, 21.55 (22.01).
NMR (400 MHz, DMSO-D_6) δ 11.91 (s, 1 H), 10.91 (s, 1H), 10.47 (s, 1H), 8.27 (s, 1H), 8.10 (d, *J* = 34.9 Hz, 1H), 7.91 (s, 1H), 7.12 (d, *J* = 126.9 Hz, 1H), 6.00 (dd, *J* = 49.9, 47.6 Hz, 1H), 3.32 (q, *J* = 6.9 Hz, 4H), 1.09 (t, *J* = 7.0 Hz, 6H).

Complex **4**, $[Zn(L4)(HL4)]NO_3$

An amount of 0.110 g (1 mmol) of 2-hydrazinopyrazine was added to 0.156 g (1 mmol) of 5-chlorosalicylaldehyde in 20 mL of 1:1 methanol/acetonitrile and stirred for 10 min. To this 0.149 g (0.5 mmol) of $Zn(NO_3)_2 \bullet 6H_2O$ was added and stirred for 20 min and the solution was filtered. Yellow/orange crystals were isolated after several days of slow solvent evaporation. Isolated Yield 72 mg, 12%.

IR (cm^{-1}): 3199, 3049, 1615, 1535, 1515, 1457, 1315, 1287, 1207, 1155, 818, 711.
Elemental Analysis: Theory (Found); C, 42.36 (43.54); H, 2.75 (2.83); N, 20.21 (20.05).
^{1}H NMR (400 MHz, DMSO-D_6) δ 11.35 (s, 1H), 10.50 (s, 1H), 8.51 (dd, *J* = 36.0, 1.4 Hz, 1H), 8.30 (s, 1H), 8.21–8.07 (m, 1H), 8.01 (t, *J* = 6.5 Hz, 1H), 7.75 (t, *J* = 3.8 Hz, 1H), 7.22 (d, *J* = 2.7 Hz, 1H), 7.20 (d, *J* = 2.7 Hz, 1H), 6.89 (d, *J* = 8.7 Hz, 1H).

2.2. Computational Data Details

Geometry optimisation of **1**–**4** was performed using density functional theory (DFT) with the ωB97X [26] functional and 6-31G(d) all-electron basis set. Final energies were refined using the def2-TZVP basis set [27], along with time-dependent DFT (TDDFT) calculations. All calculations were performed with the Q-Chem software [28].

3. Results

3.1. Structural Analysis

All four complexes were isolated and collected in moderate to low yields after several days of slow solvent evaporation. Isolating high-quality single crystals was challenging; as a result, only complex **3** was isolated with crystals of sufficient quality to obtain a structure using single-crystal X-ray diffraction (SC-XRD) techniques. We believe the numerous intermolecular interactions that occur between complexes facilitate aggregation and cause the system to form microcrystalline material unsuitable for SC-XRD.

Complex **3** crystallises in the monoclinic *C2/c* space group with an asymmetric unit consisting of two crystallographically independent Zn(II) complexes, two nitrate anions and one water molecule. Two highly disordered solvent molecules in the asymmetric unit, which were consistent with two water

molecules, were excluded using the solvent mask function in Olex2. The coordination environment of each complex consisted of two tridentate ligands with the pyrazine nitrogen, imine nitrogen and the oxygen of the phenol as the ligating atoms (Figure 2). This resulted in a $N_4O_2^-$ ligand sphere, as there is both a phenol (Zn1-O1, Zn2-O3) and phenolate (Zn1-O2, Zn2-O4) donor. A nitrate anion balancing the Zn(II) charge is hydrogen-bonded to the hydrazinyl proton on the ligand backbone. The effect of the protonation can be observed in the two Zn-O bond lengths. The phenol oxygen bonds (Zn1-O1, Zn2-O3) have lengths of 2.1595(14) and 2.1562(14) Å, respectively, while the phenolate bonds (Zn1-O2, Zn2-O4) have lengths of 2.0161(14) and 2.0419(13) Å, respectively. A list of metal–ligand bond lengths is shown in Table 1.

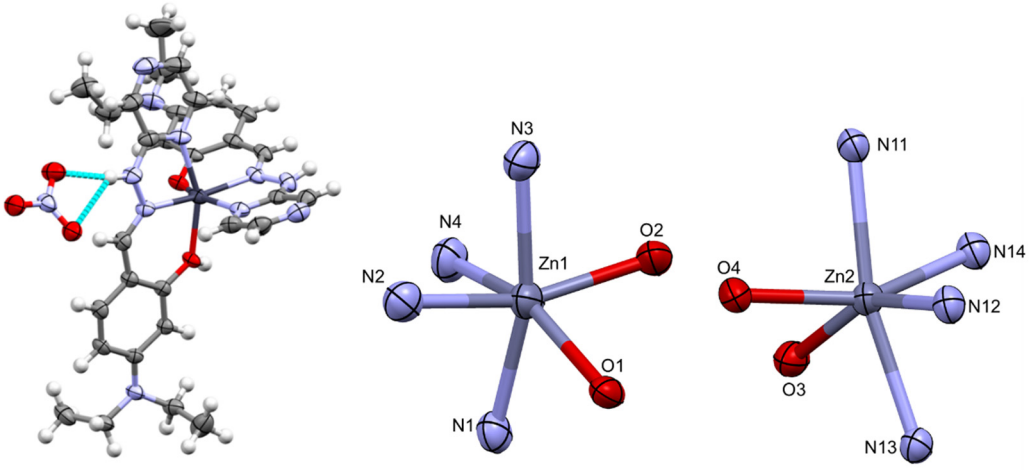

Figure 2. (**left**) Molecular structure of complex **3**, [Zn(L3)(HL3)]NO_3·3H_2O (ellipsoids at 50% probability and water omitted for clarity). (**right**) Coordination sphere of complex **3**.

Table 1. Bond lengths for both crystallographically independent Zn complexes.

Bond Type	Atoms	Length (Å)	Atoms	Length (Å)
Phenol	Zn1-O1	2.1595(14)	Zn2-O3	2.1562(14)
Phenolate	Zn1-O2	2.0161(14)	Zn2-O4	2.0419(13)
Imine	Zn1-N1	2.1123(18)	Zn2-N11	2.1405(16)
Pyrazine	Zn1-N2	2.1366(19)	Zn2-N12	2.1303(17)
Imine	Zn1-N3	2.1187(18)	Zn2-N13	2.1572(16)
Pyrazine	Zn1-N4	2.1722(18)	Zn2-N14	2.1330(16)

The presence of the mixed phenol/phenolate ligand set allows for dimerisation of the Zn complexes via hydrogen bonding (Figure 3). The dimer is formed between the two crystallographically independent Zn complexes. This dimerisation has also been observed in similar phenol/phenolate systems [29,30]. The diethylamino substituents are disordered, therefore acting as a steric buffer to stop π–π interactions between the ligands or further supramolecular polymerisation that could lead to ACQ.

Several hydrogen bond interactions take place within the lattice of complex **3**. The main interactions are between the hydrazinyl proton on the ligand, the spectator nitrate anion and water molecules. The hydrazinyl proton bonds to the oxygen of the water molecule which in turn bonds to two nitrate anions, where the motif is mirrored, resulting in a noncovalent polymeric chain (Figure 4). Here we see another "insulating" effect within the lattice as the mixture of anions and solvents isolate each of the dimers from each other in the lattice, further impeding possible ACQ.

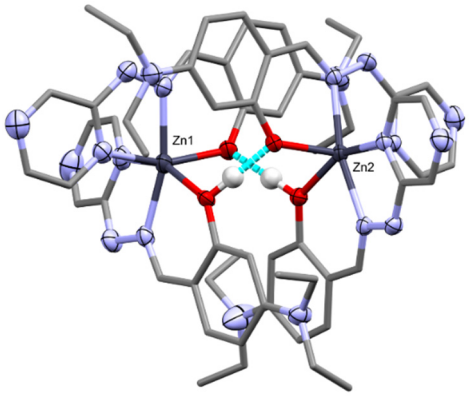

Figure 3. Hydrogen-bonded dimerisation of Zn(II) complexes between the phenol/phenolate donor sets. Hydrogen bonds in blue; heteroatoms and metal highlighted for clarity.

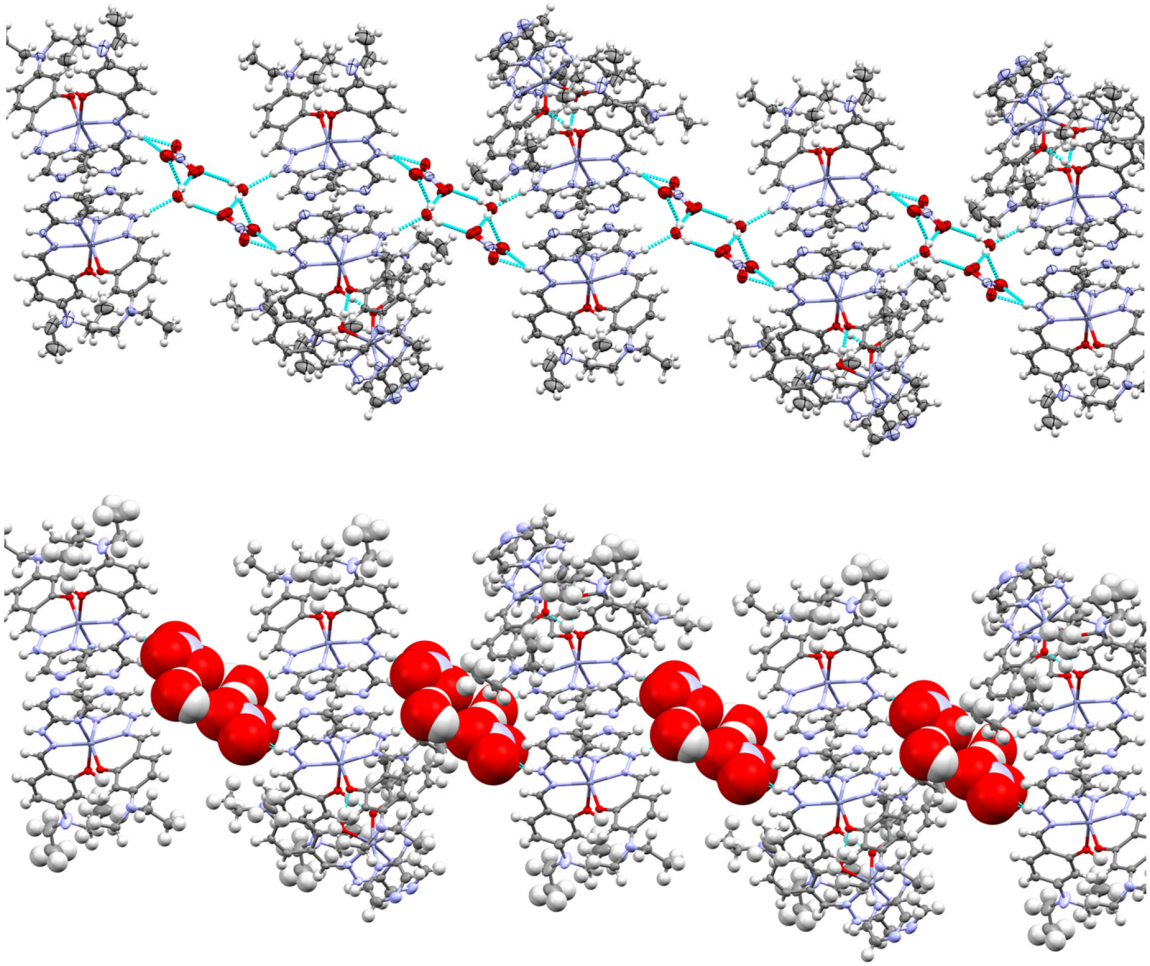

Figure 4. Formation of a noncovalent polymeric chain between the hydrazinyl protons, spectator nitrate anion and water molecules (**top**). The "insulating" effect of the water and anions is highlighted with a space-filled model (**bottom**).

3.2. ^{1}H-NMR Analysis

^{1}H-NMR studies in DMSO-d_6 were performed for each of the ligands, complexes (**1**–**4**) and a reaction of 1 equivalent of the ligand with 0.25 equivalents of the Zn salt to monitor the changes in proton environment of the ligand due to coordination (Figure 4). The common feature observed is the retention of the phenol proton from pure ligand to complex. The peak (11–12 ppm) exhibits

some shifting and broadening which can be ascribed to the effect of coordination to the zinc ion and hydrogen bonding that takes place between the phenol/phenolate donors as seen in the crystal structure of complex **3**. The singlet peak at ca. 10 ppm is the hydrazinyl proton and exhibits the broadening in the same manner as the phenol proton (Figure 5).

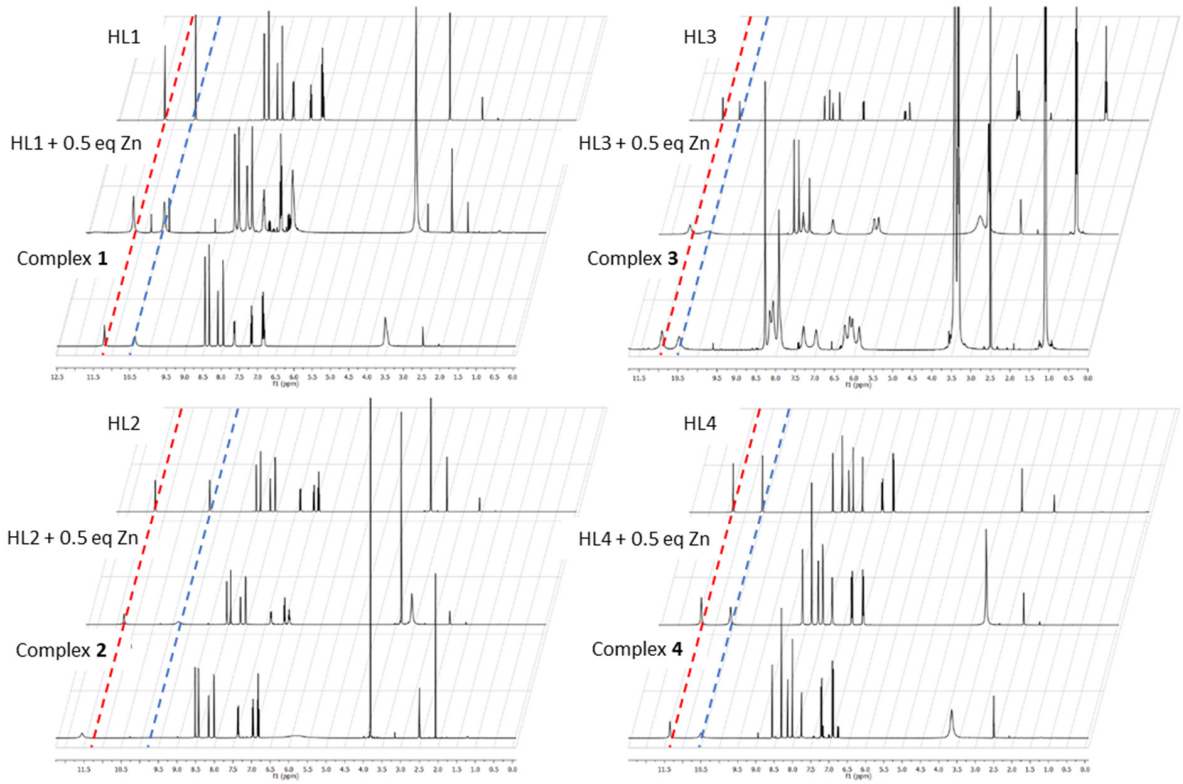

Figure 5. Stacked ^{1}H-NMR spectra for the complexes **1**–**4** featuring ligand only, a 1:1 reaction between Lx/Zn and the final complex. The red bar highlights the change in phenol proton environment and the blue bar highlights the change in hydrazinyl proton environment. Synthesis of **1**, **top left**; synthesis of **2**, **bottom left**; synthesis of **3, top right**; synthesis of **4**, **bottom right**.

In all cases, the broadening of the phenol proton and hydrazinyl proton peaks occurred upon the addition of zinc. It can thus be deduced that the complex formation goes hand in hand with the appearance of strong noncovalent interactions. The similarity of the changes in the proton environments gives some evidence that all four complexes have similar coordination and structural motifs regardless of the starting aldehyde used in the synthesis.

3.3. Electronic Absorption Analysis

UV-Vis absorption was performed to probe the coordination ability of the ligands towards Zn(II). Titrimetric experiments between the ligands, L1–L4, and Zn(II) revealed similar characteristics for all complexes, namely an increase in the π–π* band associated with the phenyl ring and a decrease in the π–π* bands associated with the pyrazine ring, relative to the starting ligand. An increase in bands related to metal-to-ligand charge-transfer (MLCT) was observed in spectra of 1–4, indicating the formation of the complex (Figures S1–S4 in the Supplementary Materials). All four complexes exhibited similar spectral features. Paired with the ^{1}H-NMR data, we propose that all complexes share a similar geometrical structure.

3.4. Luminescence Analysis

Due to the attractive luminescent character of Zn(II), we investigated the fluorescence of complexes **1**–**4** in acetonitrile solution. However, very little or negligible emission was detected over several

measured excitation wavelengths (Figure 6). To investigate the possibility of AIE, emission spectra were taken in a mixture of water and acetonitrile; however, no change was observed in the fluorescence properties of the system.

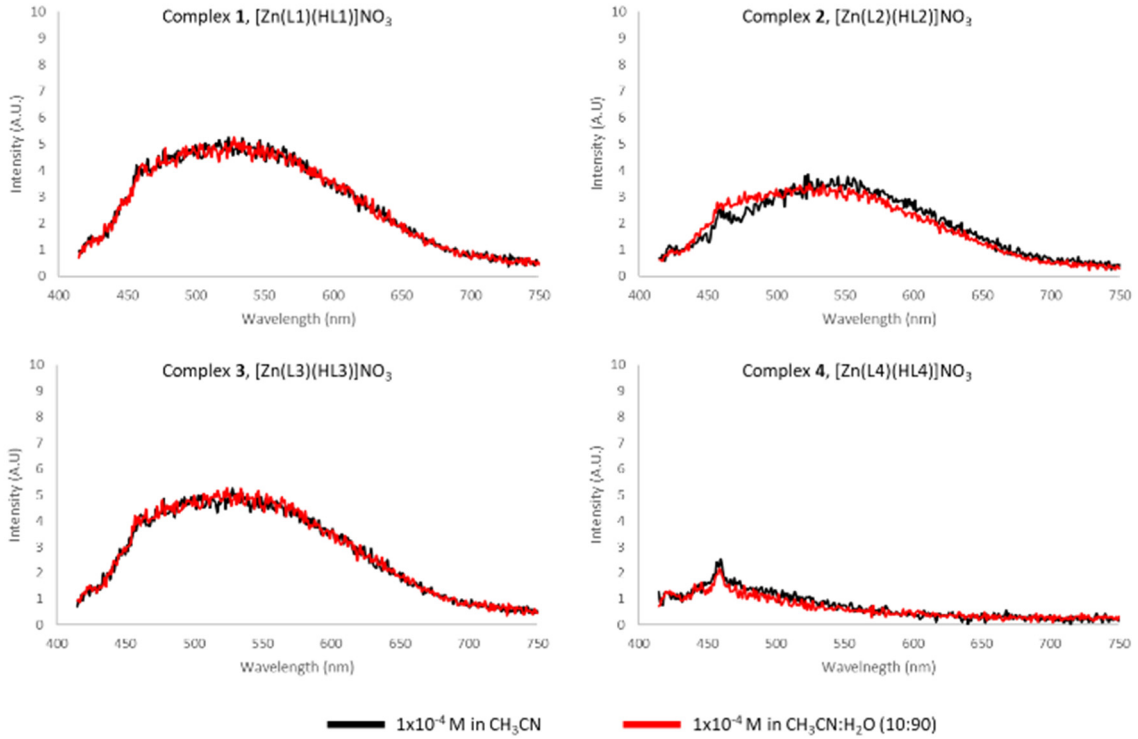

Figure 6. Emission spectra for complexes **1–4**, in CH_3CN (black) and 10:90 CH_3CN/H_2O (red). Excitation at 405 nm.

Significant emission was detected in the solid phase. Using an excitation wavelength of 405 nm, complexes **1–4** were analysed over the range of 415 to 750 nm (Figure 7). The λ_{max} values for emission for complexes **1–4** were 506, 531, 592 and 506 nm, respectively.

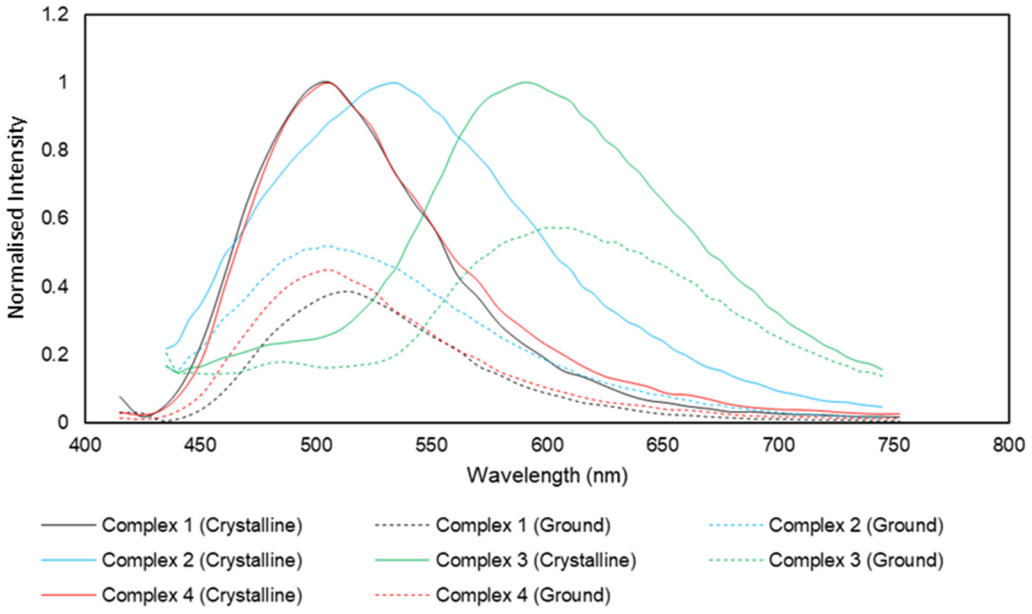

Figure 7. Normalised solid-state emission from complexes **1–4** using an excitation wavelength of 405 nm.

Crystallinity can be a deciding factor in the intensity of the fluorescence observed in CIEE systems. To probe the effect of crystallinity on the fluorescent properties, samples of complexes **1–4** were ground in a mortar and pestle for ~1 min and then analysed alongside the crystalline analogue. The spectra for the ground samples were normalised to the crystalline emission values to give a better idea of possible shifts.

From the spectra, it can be clearly observed that a significant decrease in intensity occurs in all cases. Complexes **1–4** exhibit decreases of 62%, 48%, 42% and 55%, respectively.

There are small observable shifts in the emission wavelength of each complex as well as a significant decrease in quantum yield (φ), relative to sodium salicylate (NaSal; φ = 0.60) [31,32] (Table 2).

Table 2. Comparison of crystalline complex λ_{max} and ground complex λ_{max}.

Complex	1	2	3	4
Crystalline λ_{max}	506 nm	531 nm	592 nm	506 nm
φ Rel. to NaSal	0.04	0.21	0.44	0.05
Ground λ_{max}	515 nm	505 nm	600 nm	506 nm
φ Rel. to NaSal	0.01	0.13	0.20	0.02

Complexes **1** and **3** respond to the change in crystallinity with a decrease in fluorescence intensity coupled with a bathochromic shift. Complex **2** presents the decrease coupled with a hypsochromic shift, while complex **4** exhibits a decrease in intensity only. The bathochromic shifts are approximately 10 nm shifts whereas the hypsochromic shift is nearly three times stronger at 26 nm. This type of mechanochromism can derive from the changing of internal interactions as was observed in the lattice of complex **3**. No evidence of changes in luminescent character was observed with a variation of pH.

3.5. Theoretical Analysis

Density functional theory (DFT) calculations, using the ωB97X functional [26] and def2-TZVP all-electron basis set [27], were performed to investigate the effect of the substituent on the HOMO and LUMO for each of the complexes for **1–4** (Figure 8). In all cases, the model of the complex reflected a gas-phase single complex and anion. This gives insight into the HOMO and LUMO levels but may not reflect the crystallised complex due to packing and noncovalent interactions.

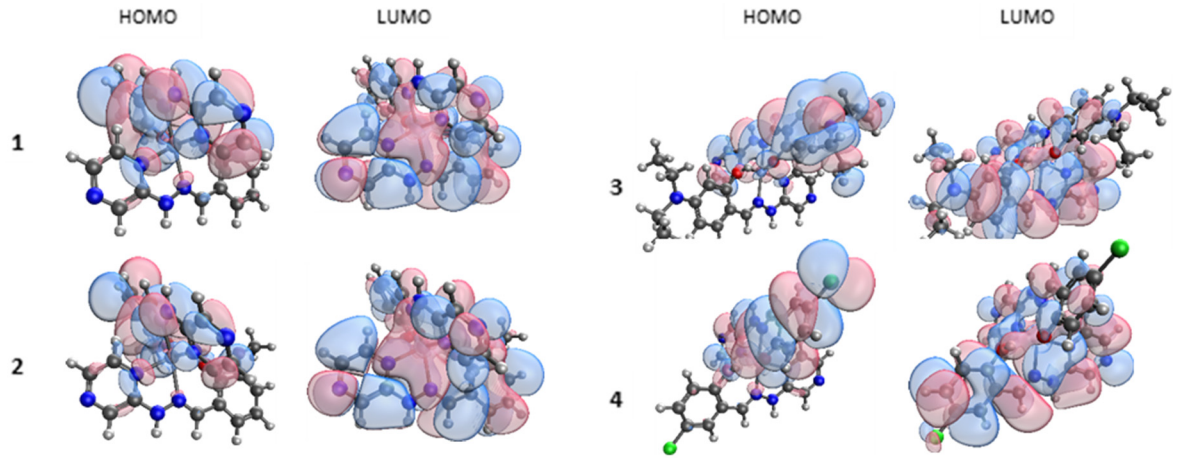

Figure 8. DFT calculated HOMOs and LUMOs for complexes **1–4**.

In each case, the HOMO is centred on the ligand with the phenolate coordination mode and on to the Zn metal centre. All four LUMOs have strong π* character and are centred across the whole complex, in contrast to the HOMOs. The TDDFT results indicate a π*–π transition is responsible for the observed luminescence, as these are the transitions observed for the absorption.

The calculated HOMO and LUMO energies in eV for the gas-phase complex are shown in Figure 9. This approach was chosen so that the direct substituent effect on the electronic structure of each complex could be understood. Complexes **2** and **3** have smaller HOMO–LUMO gaps at 6.20 and 6.26 eV, respectively. This could be attributed to the electron-donating nature of the ligand used. The lower energy barrier between the HOMO and LUMO (vs. **1** and **3**) correlates qualitatively with the lower energy emission energies of complexes **2** and **3** vs. **1** and **3** and could help in designing ways to tune these complexes to get a variety of emission wavelengths. While crystal-packing effects clearly alter the quantitative picture (indeed, the transitions observed experimentally are much lower in energy than the gas-phase calculated HOMO–LUMO gaps), the qualitative picture of substituent electronic effects will still be important when the understanding of the tuning of the emission is required.

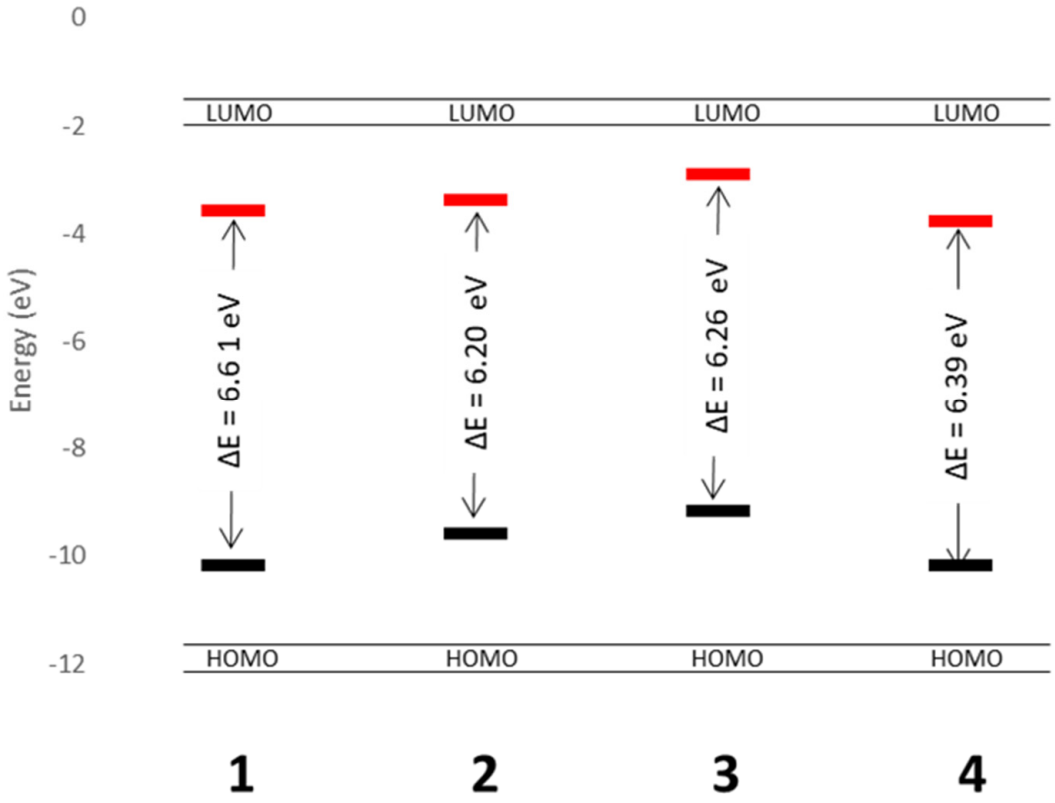

Figure 9. Energy level diagram of the calculated HOMOs and LUMOs for complexes **1**–**4**.

4. Discussion

We have synthesised four novel CIEE active Zn(II) Schiff base complexes and analysed the fluorescent properties using experimental and theoretical methods. To date, the majority of CIEE active species have poorly understood mechanisms of fluorescence. The hydrogen-bonded dimer and anion/solvent-based noncovalent interactions may give the rigidity needed to inhibit relaxation through molecular flexibility and therefore stop nonradiative decay.

We propose that the coupling of these properties, with a lack of obvious π–π interactions, is responsible for the lack of ACQ in the crystalline phase. The degree of crystallinity plays an integral role in the fluorescence intensity and gives possible insight into the lack of fluorescence in solution, where the interference of the solvent in this hydrogen-bonded network, along with the complete loss of lattice-induced molecular rigidity, may be a leading cause of fluorescence quenching. The emission wavelengths of the complexes **1**–**4** are qualitatively related to the electronic nature of the complex with the electron-donating-based ligands, L2 and L3, resulting in bathochromic shifts, compared to the unsubstituted ligand. This study yields some insight into the ability to tune the emission wavelength and possible mechanism of CIEE for these and related complexes.

Supplementary Materials: The electronic supplementary material is available online at http://www.mdpi.com/2071-1050/12/22/9599/s1. Structure of 3 deposited at www.ccdc.cam.ac.uk (CCDC 1916713).

Author Contributions: Investigation and data curation, D.J.L.G. and N.C.; conceptualisation, investigation, manuscript editing, D.R.; supervision, conceptualisation, manuscript drafting, A.J.F. All authors have read and agreed to the published version of the manuscript.

Funding: This research received no external funding.

Acknowledgments: D.J.L.G., N.C. and D.R. would like to thank Nottingham Trent University (NTU) for support. A.J.F. would like to thank Sheffield Hallam University for support. D.R. also thanks NTU for access to the Hamilton High Performance Computing facility. The authors would like to thank Kathryn Kroon and Graham Hickman for technical support for the solid-state fluorimetry.

Conflicts of Interest: The authors declare no conflict of interest.

References

1. Dumur, F. Zinc complexes in OLEDs: An overview. *Synth. Met.* **2014**, *195*, 241–251. [CrossRef]
2. Ravelli, D.; Dondi, D.; Fagnoni, M.; Albini, A. Photocatalysis. A multi-faceted concept for green chemistry. *Chem. Soc. Rev.* **2009**, *38*, 1999. [CrossRef]
3. Gokel, G.W.; Leevy, W.M.; Weber, M.E. Crown ethers: Sensors for ions and molecular scaffolds for materials and biological models. *Chem. Rev.* **2004**, *104*, 2723–2750. [CrossRef]
4. Yue, Y.-K.; Yin, C.-X.; Huo, F.-J. Highly sensitive and selective fluorescent probe for determination of Cu(II) in aqueous solution. *J. Coord. Chem.* **2014**, *67*, 2039–2047. [CrossRef]
5. De Silva, A.P.; McClenaghan, N.D. Molecular-Scale Logic Gates. *Chem. Eur. J.* **2004**, *10*, 574–586. [CrossRef] [PubMed]
6. Hong, Y.; Lam, J.W.Y.; Tang, B.Z. Aggregation-induced emission. *Chem. Soc. Rev.* **2011**, *40*, 5361–5388. [CrossRef] [PubMed]
7. Friend, R.H.; Gymer, R.W.; Holmes, A.B.; Burroughes, J.H.; Marks, R.N.; Taliani, C.; Bradley, D.D.C.; Dos Santos, D.A.; Brédas, J.L.; Lögdlund, M.; et al. Electroluminescence in conjugated polymers. *Nature* **1999**, *397*, 121–128. [CrossRef]
8. Saragi, T.P.I.; Spehr, T.; Siebert, A.; Fuhrmann-Lieker, T.; Salbeck, J. Spiro compounds for organic optoelectronics. *Chem. Rev.* **2007**, *107*, 1011–1065. [CrossRef]
9. Mei, J.; Leung, N.L.C.; Kwok, R.T.K.; Lam, J.W.Y.; Tang, B.Z. Aggregation-Induced Emission: Together We Shine, United We Soar! *Chem. Rev.* **2015**, *115*, 11718–11940. [CrossRef]
10. Dong, Y.; Lam, J.W.Y.; Qin, A.; Li, Z.; Sun, J.; Sung, H.H.-Y.; Williams, I.D.; Tang, B.Z. Switching the light emission of (4-biphenylyl)phenyldibenzofulvene by morphological modulation: Crystallization-induced emission enhancement. *Chem. Commun.* **2007**, 40–42. [CrossRef]
11. Qian, L.; Tong, B.; Shen, J.; Shi, J.; Zhi, J.; Dong, Y.; Yang, F.; Dong, Y.; Lam, J.W.Y.; Liu, Y.; et al. Crystallization-Induced Emission Enhancement in a Phosphorus-Containing Heterocyclic Luminogen. *J. Phys. Chem. B* **2009**, *113*, 9098–9103. [CrossRef] [PubMed]
12. Tong, J.; Wang, Y.J.; Wang, Z.; Sun, J.Z.; Tang, B.Z. Crystallization-Induced Emission Enhancement of a Simple Tolane-Based Mesogenic Luminogen. *J. Phys. Chem. C* **2015**, *119*, 21875–21881. [CrossRef]
13. Jin, Y.; Xu, Y.; Liu, Y.; Wang, L.; Jiang, H.; Li, X.; Cao, D. Synthesis of novel diketopyrrolopyrrole-based luminophores showing crystallization-induced emission enhancement properties. *Dyes Pigments* **2011**, *90*, 311–318. [CrossRef]
14. Wang, Z.; Wang, T.; Zhang, C.; Humphrey, M.G. Efficient crystallization-induced emission in fluorenyl-tethered carboranes. *Phys. Chem. Chem. Phys.* **2017**, *19*, 12928–12935. [CrossRef]
15. Gayen, C.; Goswami, U.; Gogoi, K.; Basu, S.; Paul, A. Crystallization-Induced Emission Enhancement of Nanoclusters and One-Step Conversion of "Nanoclusters to Nanoparticles" as the Basis for Intracellular Logic Operations. *ChemPhysChem* **2019**, *20*, 953–958. [CrossRef]
16. Guieu, S.; Cardona, F.; Rocha, J.; Silva, A.M.S. Tunable Color of Aggregation-Induced Emission Enhancement in a Family of Hydrogen-Bonded Azines and Schiff Bases. *Chem. Eur. J.* **2018**, *24*, 17262–17267. [CrossRef]
17. Park, S.; Kwon, J.E.; Park, S.-Y.; Kwon, O.-H.; Kim, J.K.; Yoon, S.-J.; Chung, J.W.; Whang, D.R.; Park, S.K.; Lee, D.K.; et al. Crystallization-Induced Emission Enhancement and Amplified Spontaneous Emission from a CF3-Containing Excited-State Intramolecular-Proton-Transfer Molecule. *Adv. Opt. Mater.* **2017**, *5*, 1700353. [CrossRef]

18. Le Bras, L.; Chaitou, K.; Aloïse, S.; Adamo, C.; Perrier, A. Aggregation-caused quenching: Versus crystallization induced emission in thiazolo[5,4-b] thieno[3,2-e] pyridine (TTP) derivatives: Theoretical insights. *Phys. Chem. Chem. Phys.* **2019**, *21*, 46–56. [CrossRef]
19. Burlov, A.S.; Vlasenko, V.G.; Koshchienko, Y.V.; Makarova, N.I.; Zubenko, A.A.; Drobin, Y.D.; Fetisov, L.N.; Kolodina, A.A.; Zubavichus, Y.V.; Trigub, A.L.; et al. Synthesis, characterization, luminescent properties and biological activities of zinc complexes with bidentate azomethine Schiff-base ligands. *Polyhedron* **2018**, *154*, 65–76. [CrossRef]
20. Naskar, B.; Modak, R.; Maiti, D.K.; Drew, M.G.B.; Bauzá, A.; Frontera, A.; Das Mukhopadhyay, C.; Mishra, S.; Das Saha, K.; Goswami, S. A Schiff base platform: Structures, sensing of Zn(II) and PPi in aqueous medium and anticancer activity. *Dalton Trans.* **2017**, *46*, 9498–9510. [CrossRef]
21. Xie, Y.Z.; Shan, G.G.; Li, P.; Zhou, Z.Y.; Su, Z.M. A novel class of Zn(II) Schiff base complexes with aggregation-induced emission enhancement (AIEE) properties: Synthesis, characterization and photophysical/electrochemical properties. *Dyes Pigments* **2013**, *96*, 467–474. [CrossRef]
22. Chakraborty, S.; Bhattacharjee, C.R.; Mondal, P.; Prasad, S.K.; Rao, D.S.S. Synthesis and aggregation behaviour of luminescent mesomorphic zinc(ii) complexes with "salen" type asymmetric Schiff base ligands. *Dalton Trans.* **2015**, *44*, 7477–7488. [CrossRef] [PubMed]
23. Hui, J.K.H.; Yu, Z.; MacLachlan, M.J. Supramolecular assembly of zinc salphen complexes: Access to metal-containing gels and nanofibers. *Angew. Chem. Int. Ed.* **2007**, *46*, 7980–7983. [CrossRef] [PubMed]
24. Consiglio, G.; Failla, S.; Oliveri, I.P.; Purrello, R.; Di Bella, S. Controlling the molecular aggregation. An amphiphilic Schiff-base zinc(II) complex as supramolecular fluorescent probe. *J. Chem. Soc. Dalton Trans.* **2009**, 10426–10428. [CrossRef] [PubMed]
25. Al Rasbi, N.K.; Adams, H.; Alshabibi, I.; Alamri, F. Structure, aggregation and spectroscopic properties of self-assembled Zn(II) Schiff base complexes. *J. Photochem. Photobiol. A Chem.* **2014**, *285*, 37–43. [CrossRef]
26. Da Chai, J.; Head-Gordon, M. Systematic optimization of long-range corrected hybrid density functionals. *J. Chem. Phys.* **2008**, *128*, 084106. [CrossRef]
27. Weigend, F.; Ahlrichs, R. Balanced basis sets of split valence, triple zeta valence and quadruple zeta valence quality for H to Rn: Design and assessment of accuracy. *Phys. Chem. Chem. Phys.* **2005**, *7*, 3297–3305. [CrossRef]
28. Shao, Y.; Gan, Z.; Epifanovsky, E.; Gilbert, A.T.B.; Wormit, M.; Kussmann, J.; Lange, A.W.; Behn, A.; Deng, J.; Feng, X.; et al. Advances in molecular quantum chemistry contained in the Q-Chem 4 program package. *Mol. Phys.* **2015**, *113*, 184–215. [CrossRef]
29. Stefankiewicz, A.R.; Wałęsa-Chorab, M.; Szcześniak, H.B.; Patroniak, V.; Kubicki, M.; Hnatejko, Z.; Harrowfield, J. Grid-corner analogues: Synthesis, characterisation and spectroscopic properties of meridional complexes of tridentate NNO Schiff-base ligands. *Polyhedron* **2010**, *29*, 178–187. [CrossRef]
30. Gusev, A.; Shul'gin, V.; Braga, E.; Zamnius, E.; Starova, G.; Lyssenko, K.; Eremenko, I.; Linert, W.; Shul'gin, V.; Braga, E.; et al. Luminescent properties of zinc complexes of 4-formylpyrazolone based azomethine ligands: Excitation-dependent emission in solution. *J. Lumin.* **2018**, *202*, 370–376. [CrossRef]
31. Al-Kuhaili, M.F. A study of the fluorescent properties of spin-coated sodium salicylate thin films. *J. Lumin.* **2006**, *117*, 209–216. [CrossRef]
32. Kristianpoller, N.; Knapp, R.A. Some Optical Properties of Sodium Salicylate Films. *Appl. Opt.* **1964**, *3*, 915–918. [CrossRef]